

Article

# Concentration and Dilution of Ultrafine Bubbles in Water

Shunya Tanaka <sup>1</sup>, Yuri Naruse <sup>1</sup>, Koichi Terasaka <sup>2,\*</sup>  and Satoko Fujioka <sup>2</sup>

<sup>1</sup> School of Science for Open and Environmental Systems, Graduate School of Science and Technology, Keio University, 3-14-1 Hiyoshi, Kohoku-ku, Yokohama, Kanagawa 223-8522, Japan; wajunsan@keio.jp (S.T.); yuuri275@keio.jp (Y.N.)

<sup>2</sup> Department of Applied Chemistry, Faculty of Science and Technology, Keio University, 3-14-1 Hiyoshi, Kohoku-ku, Yokohama, Kanagawa 223-8522, Japan; fujioka@aplc.keio.ac.jp

\* Correspondence: terasaka@aplc.keio.ac.jp; Tel.: +81-45-566-1575

Received: 15 October 2020; Accepted: 3 November 2020; Published: 5 November 2020



**Abstract:** Submicron-sized bubbles are now officially called ultrafine bubbles (UFBs) by the international standard. The concentration of UFBs is generally low ( $<10^9$  particles/mL;  $<0.001$  vol%) compared to other colloidal dispersions. To overcome this practical problem, we concentrated UFBs in ultrapure water prepared by a commercial UFB generator and quantified the effect of rotary evaporation of the dispersion media on the stability of UFBs. The UFB dispersions were characterized by a particle tracking analysis (PTA) instrument. The experimental results showed that the UFBs can be diluted and concentrated without changing the size distribution and there was little or no loss of UFBs. By using a rotary evaporator, UFB dispersions were about 30-fold concentrated and the resultant number concentration reached over  $3 \times 10^{10}$  particles/mL. Increasing the concentration of UFBs allowed for satisfactory dynamic light scattering (DLS) measurements. The differences among the three algorithms for analyzing the raw data, i.e., autocorrelation function, obtained by DLS are discussed, along with the characteristics of the particle size distribution derived from each algorithm.

**Keywords:** nanobubble; particle tracking analysis; dynamic light scattering; rotary evaporator; number concentration; size distribution; NNLS; CONTIN; Marquardt

## 1. Introduction

In recent years, industrial use of submicron-sized bubbles has been increasing. Accordingly, since 2017, international standards related to the bubbles have been published annually by the International Organization for Standardization (ISO). According to the standard, these colloidal bubbles are referred to as not “nanobubbles” or “bulk nanobubbles” but “ultrafine bubbles.” Therefore, in this study, we will refer to the submicron-sized bubbles as ultrafine bubbles (UFBs) [1].

The greatest mystery of UFB lies in its extraordinary stability. The ISO standard [1] defines UFB as a bubble with a volume equivalent diameter of less than 1  $\mu\text{m}$ . However, due to its small size, the existence of UFBs is not supported by classical theories. For instance, Epstein and Plesset’s theory predicts a lifetime of less than a second for a 1- $\mu\text{m}$  bubble [2]. Nevertheless, many experimental studies have reported that UFBs can remain stable for weeks to months [3]. At present, no one has seemingly unraveled this contradiction clearly, and it has caused a great deal of controversy for researchers working on UFBs.

For example, Alheshibri and Craig [4–6] insist that the particles called UFBs or nanobubbles are not gas-filled bubbles. Their conclusions are based on the results of particle density measurements and compressibility. They measured the particle density of the UFBs using a device called resonant mass measurement (RMM), which can measure the buoyant mass and predict the density of particles

in a liquid dispersion. The measured densities of the particles were about  $0.9 \text{ g/cm}^3$ , which is obviously larger than the density of a gas, i.e.,  $0.001 \text{ g/cm}^3$ . The other evidence was obtained using the dynamic light scattering (DLS) technique with a pressurizable cuvette cell. By using this apparatus, they demonstrated that the particles did not shrink even under an external pressure of 10 atm, which belies the fact that the particles are gas-filled entities.

On the contrary, Jadhav and Barigou [7] argue that UFBs and nanobubbles are indeed gas-filled particles. They used eleven different physical and chemical methods, including Cryo-SEM (scanning electron cryomicroscopy), GC-MS (gas chromatography-mass spectrometry), and ICP-MS (inductively coupled plasma mass spectrometry) to analyze the dispersions of UFBs. They reported that the dispersions prepared by three different UFB generation methods did not provide sufficient evidence that the UFBs were organic or inorganic contaminants. If the UFBs were not gaseous, the presence of the measured particles could not be explained.

In this context, a variety of analytical methods are needed to promote fundamental research on UFBs. However, the concentrations of UFBs are usually so dilute that various analyses can be challenging; typical number concentrations of UFBs are on the order of  $10^7$  particles/mL to at most  $10^9$  particles/mL, which is less than 0.001 vol% or 0.01 mM. Many analyzers have an appropriate concentration range and deviation from the range can not only result in irreproducible data but can also result in data that lead to erroneous conclusions. For example, it has been reported that the data quality of DLS is affected by the number concentration of colloidal particles [8]. This is where basic analytical operations, such as dilution and concentration, are essential.

Despite the fundamental importance, little has been reported on the dilution or concentration of UFB dispersions. A limited number of reported examples are the studies of Tuziuti et al. [9], and Jadhav and Barigou [7]. Tuziuti et al. [9] investigated the effect of dilution on the stability of UFBs. They found that the addition of degassed water altered the stability of UFBs. Regarding the process to concentrate UFB dispersion, Jadhav and Barigou [7] used a rotary evaporator to obtain high enough concentration for the analytical techniques they used. Although the effect of evaporation on the stability of UFBs was not discussed in detail, they obtained their highest concentration of UFBs of  $1.39 \times 10^{10}$  particles/mL as a result of the evaporation process. This implies that UFB dispersions were evaporable and thus may have withstood the temperature and vacuum conditions within the evaporator. Although the above two examples provide very useful insights, important aspects such as controllability of the number concentration and size distribution were outside the focus of their work.

This study is probably the first to focus solely on the very practical processes such as dilution and concentration of UFB dispersions. We investigated the effect of dilution and rotary evaporation on the stability of UFBs generated by a commercial bubble generator. The effects of each manipulation on the number concentration and size distribution were measured by particle tracking analysis (PTA). The concentrated UFB dispersions were successfully quantified by DLS, which is known to be unreliable at dilute sample concentrations. Since stable light scattering data were obtained, the choice of algorithms and resultant size distribution are also discussed in detail.

## 2. Materials and Methods

### 2.1. Generation of Ultrafine Bubbles in Ultrapure Water

Ultrafine bubbles were generated using a commercial UFB generator, ultrafine GaLF (FZ1N-02, IDEC Co., Osaka, Japan). The gas used was laboratory air filtered through a hollow fiber filter (KIC-T6, Kitz Micro Filter Co., Nagano, Japan) whose pore size was  $0.01 \mu\text{m}$ . The dispersion medium for the UFBs was purified water as described later. The gas and liquid volume flow rates of the generator were 0.7 L/min and 16.7 L/min, respectively, hence the gas-to-liquid ratio was approximately 0.04.

The system utilizes the pressurized dissolution mechanism to generate UFBs. The pressure in the pressurized dissolution tank of the generator has been kept at a gauge pressure of  $300 \pm 20 \text{ kPa}$ . This supersaturation is thought to be the source of the UFB generation [10]. However, the detailed

generation mechanism of UFBs is not known to date. A hypothesized mechanism can be found on the manufacturer's web site (IDEC Global) [11].

## 2.2. Ultrapure Water and Glassware

Water with as little contamination as possible is required for the dispersion medium, dilution of the prepared UFB dispersions, and cleaning of laboratory equipment. In this study, ultrapure water was prepared by treating tap water with a water purifier (UL-pure KE0119, Komatsu Electronics Co., Ltd., Ishikawa, Japan). The total organic carbon concentration (TOC) and electrical conductivity of the ultrapure water were less than 50 µg/L and 0.01 mS/m, respectively; the conductivity was measured by an electrical conductivity meter attached to the water purifier, and the TOC was measured by a TOC analyzer (TOC-LCSH, Shimadzu Co., Kyoto, Japan).

In order to exclude the effect of unexpected contaminants, the glassware used were newly purchased for this study, washed with neutral detergent, and rinsed thoroughly with a large amount of ultrapure water before experiments. The measurement of TOC was obtained for the ultrapure water in the beakers cleaned in this way; therefore, the residual level of organic matter due to detergent residues was negligible (TOC < 50 µg/L). This indicates that the experimental apparatuses were maintained at a very high level of cleanliness. Table 1 summarizes the values of total organic carbon concentration, electrical conductivity, liquid temperature, and dissolved oxygen concentration of the ultrapure water. The dissolved oxygen (DO) concentration and temperature were measured using a fluorescence type DO meter (Seven2Go Pro, Mettler Toledo, Greifensee, Zürich, Switzerland).

**Table 1.** Properties of the ultrapure water.

Measurand	Value
Number concentration of foreign particles [particles/mL]	$<1 \times 10^7$
Total organic carbon concentration [µg/L]	<50
Electrical conductivity [mS/m]	<0.01
Temperature [°C]	$24 \pm 2.0$
Dissolved oxygen concentration C [mg/L]	8.3–8.7
Oxygen saturation $S_{O_2}$ [%]	97–103

The measured dissolved oxygen concentration  $C$  can be normalized by the solubility  $C^*$  at the temperature and atmospheric pressure during measurement, which is expressed as follows:

$$S_{O_2} = \frac{C}{C^*} \quad (1)$$

where  $S_{O_2}$  is oxygen saturation. Thus, if the dissolved oxygen concentration is 8.5 mg/L at 25 °C and 1 atm (=101.3 kPa), the  $S_{O_2}$  is 100%. Assuming that oxygen saturation and nitrogen saturation are approximately equal,  $S_{O_2}$  can be viewed as air saturation.

## 2.3. Dilution with Air-Saturated and Degassed Water

Degassed ultrapure water for dilution was prepared by vacuum decompression at an absolute pressure of 20 kPa ( $\approx 0.2$  atm) for 30 min using a diaphragm pump (DIVAC 0.6 L, Leybold GmbH, Cologne, Germany) and an acrylic desiccator. Air-saturated ultrapure water was used as it was taken straight from the water purification system (UL-pure KE0119).

Here the dilution factor  $f$  is defined as follows:

$$\frac{1}{f} = \frac{V_0}{V_0 + V_{\text{dil}}} \quad (2)$$

where  $V_0$  is the initial sample volume and  $V_{\text{dil}}$  is the volume of diluent. Based on this equation, when a sample is diluted twofold, the dilution factor  $f$  is 2 and the concentration is halved. In this study,

the inverse of  $f$  is defined as the dilution ratio  $1/f$ ; the dilution ratio takes a maximum value of 1 when not diluted and is zero when diluted to infinity.

#### 2.4. Rotary Evaporation

UFB dispersions were concentrated using a rotary evaporator (N-1100, TOKYO RIKAKIKAI Co., Ltd., Tokyo, Japan). Figure 1 shows the appearance and schematic diagram of the evaporator. As indicated in Figure 1b, we define “concentrate” as the liquid that is concentrated by evaporation and “condensate” as the liquid condensed by the condenser.

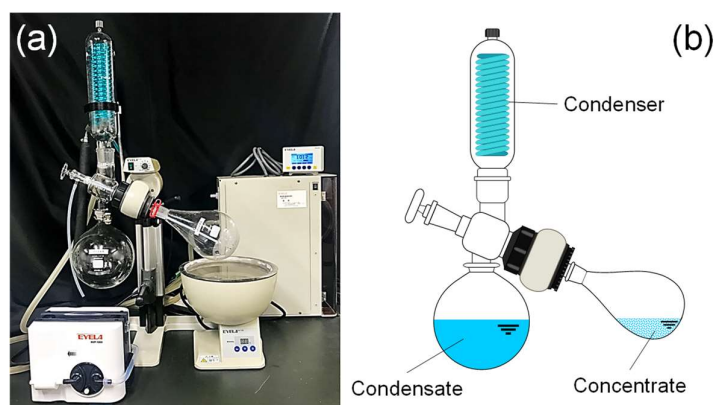


**Figure 1.** Rotary evaporation system used in this study: (a) Photo of the system; (b) Schematic showing concentrate and condensate.

The water temperature in the heating bath was 60 °C. The coolant in the concentrator was an ethylene glycol-based antifreeze, and the cooling temperature was set to −22 °C. After thoroughly rinsing the clean evaporation flask with the UFB dispersion to be concentrated, 300 mL of the dispersion was added and the concentration operation was performed at a rotation speed of 30 rpm (revolutions per minute). The decompression pressure was set at 7.0 kPa (=0.069 atm) and the time from the start of the decompression to reaching this pressure was set at 3 min.

As shown in Figure 2a, the evaporation rate, i.e., the decreasing rate of concentrate, was approximately constant at −5.3 mL/min under the present experimental conditions. Accordingly, the condensate volume also increased at a condensation rate of 5.2 mL/min (Figure 2b). The very small difference is presumably due to the loss of adhesion to the glassware.

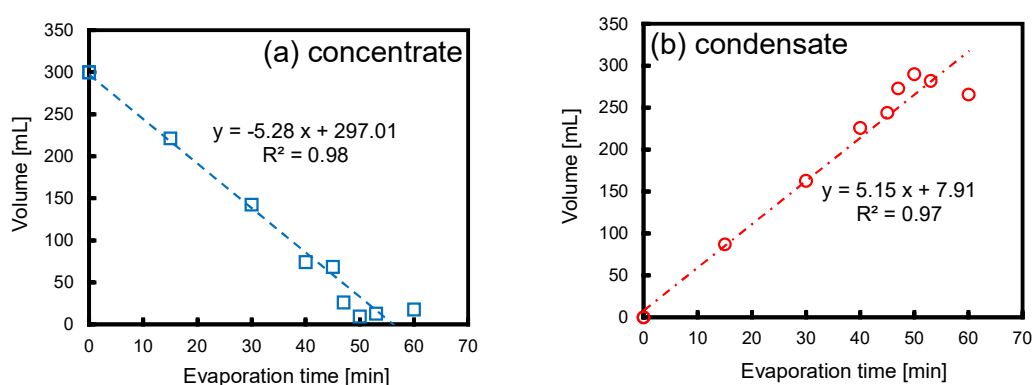


**Figure 2.** Time variation in the volume of (a) concentrate and (b) condensate under evaporation. Each data point represents an independent operation.

#### 2.5. Particle Tracking Analysis

The UFB dispersions were characterized using a particle tracking analysis (PTA) instrument (NanoSight, Malvern Ltd., Worcestershire, UK). A detailed description of PTA can be found in the

literature [12]. In brief, PTA is a method to obtain the diffusion coefficient of each particle from image analysis. The translational diffusion coefficient  $D_t$  can be calculated by Equation (3):

$$D_t = \frac{\overline{(x, y)^2}}{4t} \quad (3)$$

where  $\overline{(x, y)^2}$  is the mean square displacement of a particle in the two-dimensional plane ( $XY$ -plane) and  $t$  is the time period for the displacement. The particle diameter  $d$  can be derived by the Stokes–Einstein equation as follows:

$$d = \frac{k_B T}{3\pi\mu D_t} \quad (4)$$

where  $k_B$  is the Boltzmann constant,  $T$  is the absolute temperature,  $\mu$  is the dynamic viscosity of the dispersion. Note that it is also possible to determine the diffusion coefficient by measuring the mean square displacement in one or three dimensions. In this case, the diffusion coefficient is calculated as follows:

$$D_{t,1} = \frac{\overline{(x)^2}}{2t} \quad (5)$$

$$D_{t,3} = \frac{\overline{(x, y, z)^2}}{6t} \quad (6)$$

where  $D_{t,1}$ , and  $D_{t,3}$  are the diffusion coefficients in one and three dimensions, respectively. As noted in the ISO standard (ISO19430, Particle Tracking Analysis) [13], the particle size can be determined from the mean square displacement of the measured dimension (two dimensions in the case of the NanoSight system) by using the appropriate equation as shown above. A theoretical proof for the equations can be found in the ISO document [13].

Figure 3a shows a screenshot of a video captured by the PTA instrument used in this study. As can be seen in this figure, each particle, in this case, UFB, is detected as scattered light. The two-dimensional displacements of the particles are analyzed by the image analysis software (NTA3.2, Malvern) as shown in Figure 3b, where the trajectories of the detected particles are illustrated. The recorded displacement data are used to calculate the diameters of the particles based on Equations (3) and (4). Note that 40 trajectories are shown in Figure 3b as an example, but more than 1000 trajectories were analyzed to obtain size distributions. In addition to particle size, PTA can be used to estimate the number concentration of particles in the dispersion. Assuming that one scattered light on the imaging screen corresponds to one particle, the number concentration can be calculated from the depth of field and the area of the field of view. In the case of the NanoSight system, these values are described in the operation manual as  $\sim 10 \mu\text{m}$ , and  $\sim 100 \mu\text{m} \times \sim 80 \mu\text{m}$ , respectively.

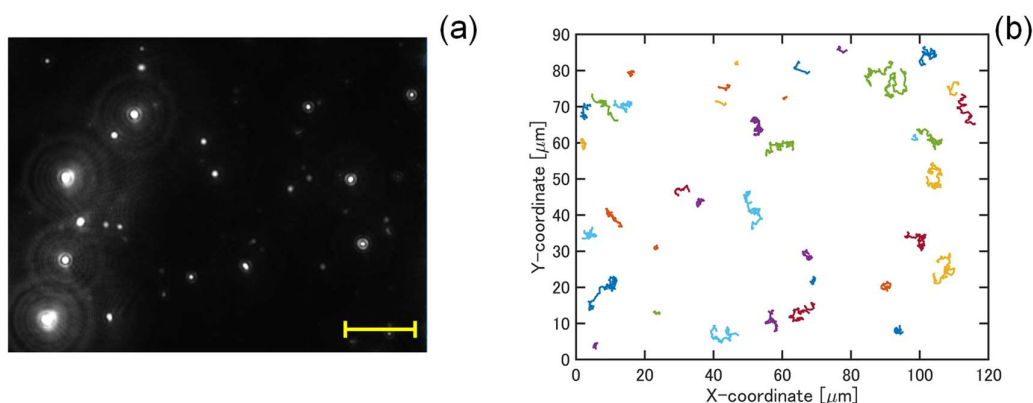


**Figure 3.** Typical PTA measurement: (a) Acquisition of scattered lights from UFBs; (b) Recorded particle trajectories. The scale bar in (a) corresponds to  $20 \mu\text{m}$ .

The PTA instrument used in this study was the NanoSight LM10 system (Malvern Ltd.). The PTA instrument is equipped with a violet laser (wavelength:  $\lambda = 405$  nm) and analytical software (NTA 3.2 Dev Build 3.2.16, Malvern Ltd.). Each PTA measurement consisted of video recording and image analysis of the videos taken. Five movies of 60 s each were taken for each measurement. The image acquisition parameter called “camera level” and the analytical parameter called “detection threshold” were 12 and 5, respectively. These parameters are known to have a significant effect on the apparent number concentration of particles and particle size [14]. In this measurement condition, when 10 particles are detected on the screen, the number concentration is equivalent to  $2.0 \times 10^8$  particles/mL. To obtain reliable size distribution, at least 1000 tracks were analyzed.

### 2.6. Dynamic Light Scattering

The concentrated UFB dispersions were measured using a dynamic light scattering (DLS) instrument (ELSZ-1200, Otsuka Electronics, Co., Ltd., Osaka, Japan). The instrument is equipped with a 70 mW and 633 nm He-Ne laser. The scattering angle is  $165^\circ$ . The optimal light scattering intensity is between  $10^4$  cps and  $10^5$  cps (photon count rate per second). This system is equipped with an attenuation filter that automatically regulates the incident light if the scattering intensity is above the range. Preliminary experiments showed that the scattering intensity of the original UFB dispersions prepared by the UFB generator was too low to be measured. Therefore, the concentrated UFB dispersions were measured and reported in this study. Each measurement consisted of 70 runs. The measurements were performed three times. As recommended by the manufacturer, the samples were filtered through a 0.42- $\mu\text{m}$  membrane filter before measurement. It should be noted that the filtration did not affect the number concentration or particle size, which was confirmed beforehand using the PTA method. In addition to the cumulant method as summarized in the ISO standard [15], the CONTIN method [16], the NNLS (non-negative least squares) method [17], and the Marquardt method [18] are implemented in the software of the DLS instrument.

## 3. Results and Discussion

### 3.1. Dilution of Ultrafine Bubble Dispersions

One of the aims of this study is to obtain high concentrations of UFBs. A higher concentration of UFBs would provide a stronger signal for a variety of analyses. However, the concentrated UFB dispersions cannot be analyzed directly in the PTA system because too high concentrations of UFBs would significantly disturb the image analysis. According to the manufacturer’s manual, the upper limit of the PTA instrument is approximately  $2 \times 10^9$  particles/mL. At higher number concentrations than the upper limit, the dispersion is required to be diluted. The effect of dilution on the stability of UFBs is shown in Figures 4 and 5.

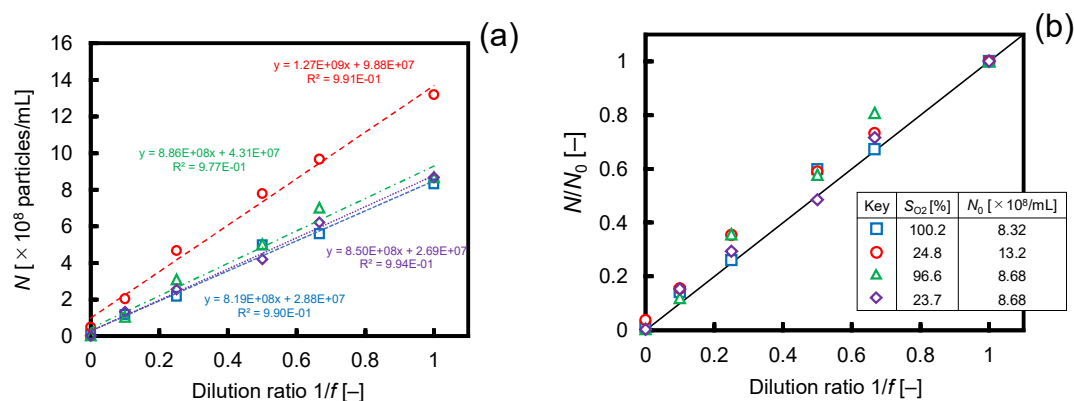


**Figure 4.** Effect of dilution on the number concentration of UFBs. (a) Raw data and (b) normalized value by the initial number concentration  $N_0$  before dilution.  $S_{O_2}$  in the legend indicates diluent  $S_{O_2}$ .

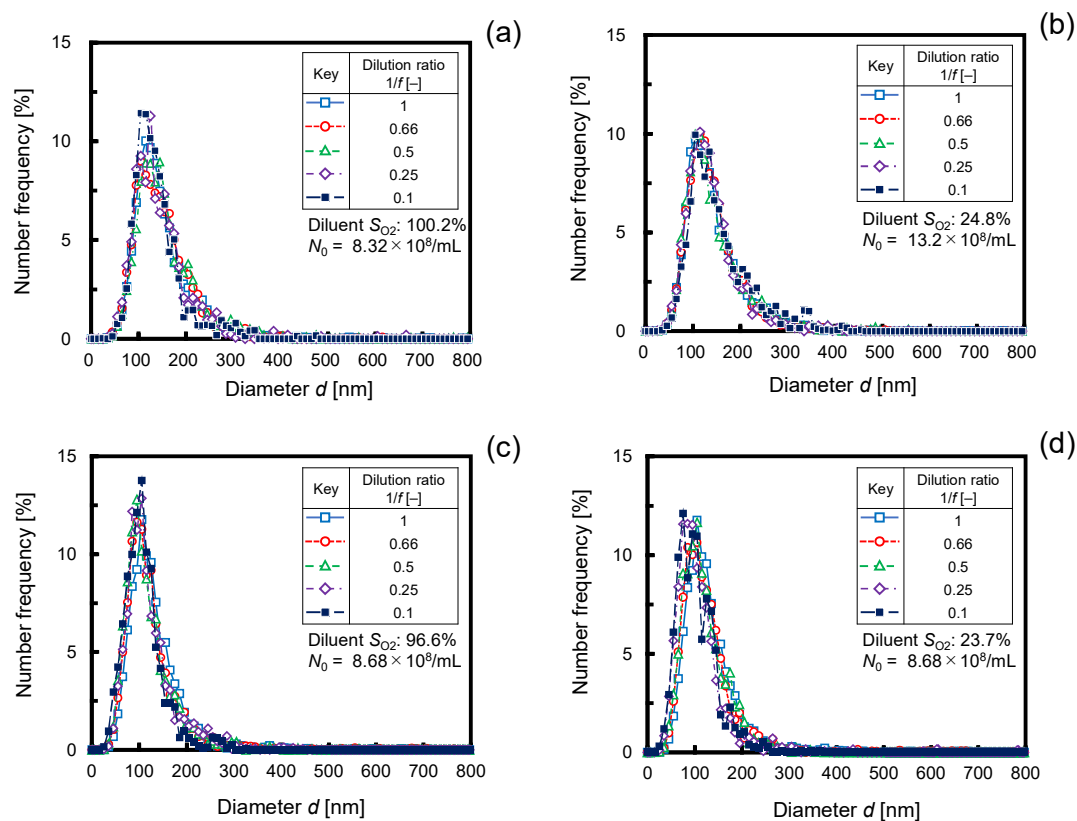


**Figure 5.** Effect of dilution on the size distribution of UFBs. (a) Untreated diluent ( $S_{O_2} = 100.2\%$ ;  $N_0 = 8.32 \times 10^8$  particles/mL). (b) Degassed diluent ( $S_{O_2} = 24.8\%$ ;  $N_0 = 13.2 \times 10^8$  particles/mL). (c) Untreated diluent ( $S_{O_2} = 96.6\%$ ;  $N_0 = 8.68 \times 10^8$  particles/mL). (d) Degassed diluent ( $S_{O_2} = 23.7\%$ ;  $N_0 = 8.68 \times 10^8$  particles/mL). The bin width is 10 nm.

Figure 4 clearly illustrates that UFB dispersions were able to be diluted in both untreated and degassed ultrapure water without loss of the stability of UFBs. As can be seen in Figure 4a, the values of the correlation coefficients  $R^2$  were greater than 0.97, indicating excellent linearity. The good linearity ensures that the UFB dispersion can be diluted to the desired concentration. Figure 4b gives a plot of  $N/N_0$ , the number concentration  $N$  normalized by the initial number concentration  $N_0$  before dilution, against the dilution ratio  $1/f$ . The solid line in the figure shows the theoretical value of  $N/N_0 = 1/f$ . Therefore, if a value of  $N/N_0$  is smaller than this solid line, it indicates that the diluted concentration is lower than the theoretical value, i.e., the stability of UFBs may have been lost. However, as is evident in the figure, almost all the data points are equal or larger than the value of the solid line. This indicates that the stability of UFBs is preserved regardless of the oxygen saturation  $S_{O_2}$  of diluent.

The results of the size distribution of UFBs also support that the stability of UFBs was not lost by dilution. Figure 5 illustrates the effect of dilution on the bubble size distribution. The number frequency distribution was calculated by dividing the number concentration of each bin (10 nm) by the total number concentration. Therefore, the sum of the height of the number frequency is equal to 100%. The normalized size distributions overlapped well; thus, the dilution was found to have little or no effect on the bubble size. Based on these experimental facts, we conclude that the number of UFBs in the dispersion can be adjusted arbitrarily by dilution while maintaining the size distribution.

Note, however, that the present results and the conclusion above are limited to the case of ultrapure water shown in Table 1. Since the dilutions in this study were performed using the pure diluent, it can be expected that the results would be different when salts and other substances are added to the diluent. For example, it has been reported that both the number of UFBs and their size are affected by changes in pH and salt concentration [19]. Therefore, attention will need to be paid to the quality of the diluent.

It should also be noted that the different initial concentrations  $N_0$  of UFBs before dilution were due to the different generation dates of the UFBs. Although the number concentrations differed according to the date of generation, the size distribution was consistent among the UFBs: the peak diameters were around 100–120 nm.

As shown in Figure 6, the oxygen saturation  $S_{O_2}$  was on the theoretical line calculated by mass balance, indicating that dilution by degassed water reduced  $S_{O_2}$  following the theory. Some may try to discuss the stability of UFBs in terms of dissolved gas concentrations, but a simple calculation shows that this is difficult to do. The molar concentration of the gas within the UFBs in water can be easily calculated from the number concentration (e.g.,  $1 \times 10^9$  particles/mL) and size (e.g., 200 nm) of UFBs to about  $0.6 \mu\text{mol/L}$ ; the ideal gas law and the increase in the bubble's internal pressure due to Laplace pressure, i.e.,  $\Delta P = 4\sigma/d$ , were taken into account, where  $\sigma$  is the surface tension. If the bubbles consist of air (21 vol% oxygen), this molar concentration can be converted to a dissolved oxygen concentration of about  $0.02 \text{ mg/L}$ . Since the resolution of the DO meter is  $0.01 \text{ mg/L}$ , we find it difficult in practice to measure the increase or decrease of UFBs with the dissolved gas concentration. For more information on the above calculation, please see Appendix A.

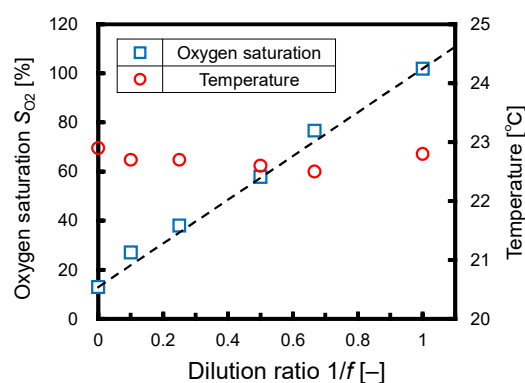


**Figure 6.** Effect of dilution on the oxygen saturation  $S_{O_2}$  and temperature of a UFB dispersion. The dashed line is the theoretical value calculated from  $S_{O_2}$  of the diluent ( $S_{O_2} = 12.9\%$ ) and the UFB dispersion ( $S_{O_2} = 101.9\%$ ).

Based on these results, which show that the UFBs prepared by the commercial generator were stable in undersaturated water, it seems to be reasonable to suspect that the UFBs are not gaseous in nature. In fact, Alheshibri and Craig [4] and Häbich et al. [20] pointed out that the particles alleged to be UFBs may be impurities in the fluids. On the contrary, Uchida et al. [21,22] reported evidence that UFBs may exist in the liquid as a gaseous bubble. They used the freeze-fracture replica method to make a replica of the UFBs and observed many holes, which were thought to be traces of the bubbles, under an electron microscope. It has also been argued that UFBs are indeed gaseous bubbles using in-situ methods such as infrared (IR) spectroscopy: Oh and Kim [23] presented IR spectral data for  $\text{CO}_2$ -UFB dispersions as evidence of gaseous bubbles. These results are contradictory and highlight the need for further experimental research. Several attempts [24,25] have been reported to explain the stability of UFBs theoretically; however, no widely accepted theory seems to be available yet.

### 3.2. Evaporation of Ultrafine Bubble Dispersions

A photograph of ultrapure water, condensate, UFB dispersion before and after evaporation is shown in Figure 7. As a result of evaporation for 54 min, the concentrated UFB dispersion (no. 4) became slightly cloudy, whereas the other samples (no. 1–3) were transparent (Figure 7a). As is clear from Figure 7b, laser irradiation makes the presence or absence of UFBs more apparent; a strong streak of the laser light can be seen in the original UFB dispersion (no. 3), and the concentrated UFB dispersion (no. 4).

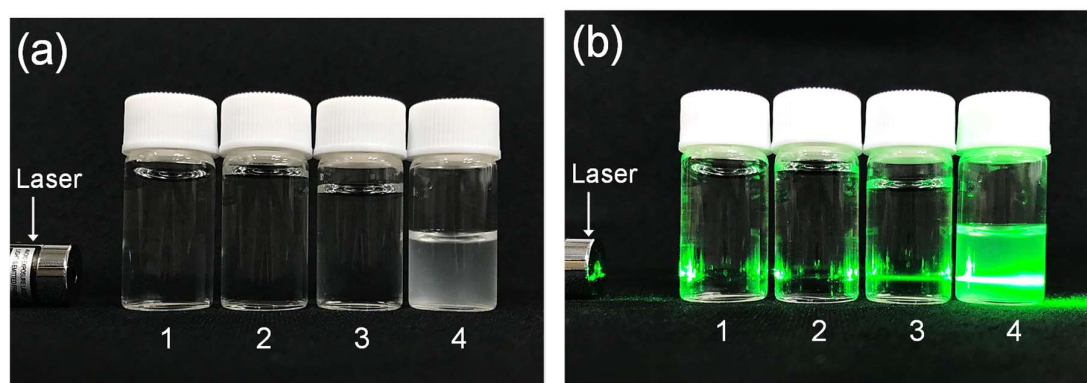


**Figure 7.** Photographs showing the samples in glass vials: (1) ultrapure water, (2) condensed water, (3) original UFB dispersion, and (4) concentrated UFB dispersion. (a) Without and (b) with illumination by a laser pointer with a power of 150 mW and a wavelength of 532 nm.

In order to confirm whether the number concentrations of UFBs were preserved in the concentrates, the concentrated UFB dispersions with different volumetric concentration ratios were quantified by the PTA instrument. Here, the volumetric concentration ratio can be defined as  $V_0/V_c$ , where  $V_0$  is the initial volume of concentrate (300 mL in this study) and  $V_c$  is the volume of the concentrate reduced by evaporation for a given time. Based on this definition, for instance, if the volume of concentrate is reduced to 1/4 ( $V_c = 1/4 V_0$ ), the volumetric concentration ratio  $V_0/V_c$  is calculated to be 4; therefore, it is a 4-fold concentration. Similarly, the number concentration ratio can be also defined as  $N/N_0$ , where  $N_0$  is the initial number concentration before evaporation and  $N$  is the number concentration after evaporation. Theoretically, if the volumetric concentration ratio  $V_0/V_c$  increases by a factor of 4, the number concentration ratio will also be the same factor; therefore, the plots of the values will show a straight line through the origin. The results of the evaporation experiments are shown in Figures 8 and 9.

It is clear from Figure 8 that the number concentration was preserved. The number concentration ratio  $N/N_0$  and volumetric concentration ratio  $V_0/V_c$  of the UFB dispersions agreed within  $\pm 8\%$ . Note that each data point shows the value of independent evaporation; therefore, the evaporation process is highly reproducible. The number concentration was concentrated up to 29.1-fold compared to the initial concentration, resulting in  $3.44 \times 10^{10}$  particles/mL. With regards to the size of UFBs as shown in Figure 9, the size distribution did not significantly change. The preservation of size distribution is advantageous for various analyses.

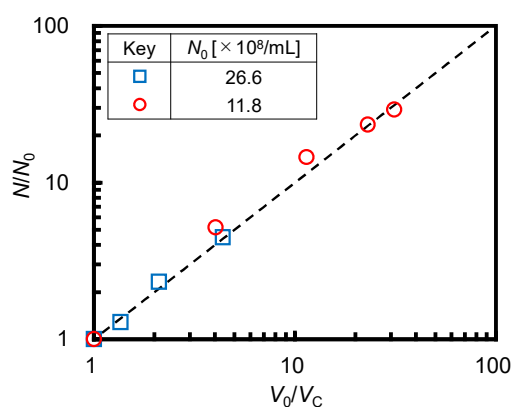


**Figure 8.** Effect of rotary evaporation on the number concentration of UFBs: number concentration ratio  $N/N_0$  vs. volumetric concentration ratio  $V_0/V_c$ . The dashed line indicates the theoretical value.

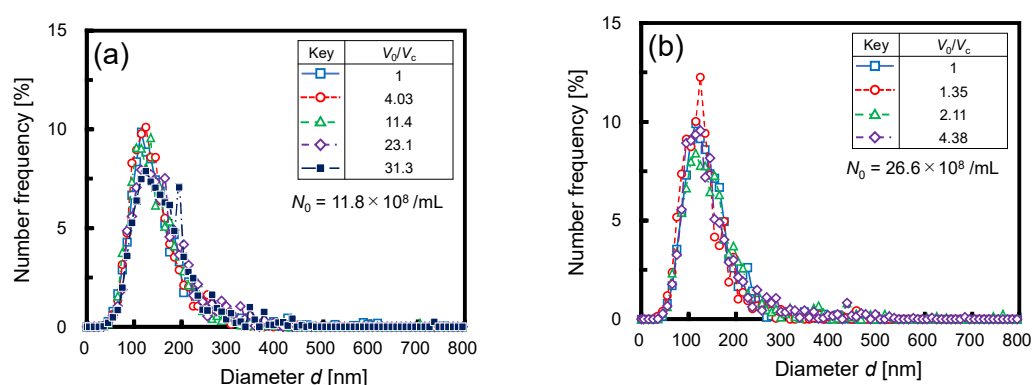


**Figure 9.** Effect of concentration using the rotary evaporator on the size distribution of UFBs. Initial concentration  $N_0$  in (a) is  $11.8 \times 10^8$  particles/mL and in (b) is  $26.6 \times 10^8$  particles/mL. The bin width is 10 nm.

Figure 10 shows a typical change in the oxygen saturation  $S_{O_2}$  and temperature of concentrate under the evaporation process. In this case, a UFB dispersion with a number concentration of about  $10^8$  particles/mL was concentrated and measured. The  $S_{O_2}$  of the concentrate dropped to less than 20% within 3 min of the start of evaporation and the temperature rose to over 35 °C. The difference between the expected values from the operating conditions (vacuum pressure of 7 kPa and heating bath temperature of 60 °C) was mainly due to the use of the probe-type dissolved oxygen meter; we measured  $S_{O_2}$  by stopping the evaporator and placing the probe in the concentrate in the evaporation flask taken out of the heating bath. This manipulation may have caused the liquid temperature to drop due to contact with the probe and the  $S_{O_2}$  to rise due to the diffusion of ambient air. The effect of the probe insertion was more pronounced at the end of evaporation, where the volume of concentrate was reduced; the increase in  $S_{O_2}$  and the drop in temperature after about 40 min from the start of evaporation were presumably due to the reduced volume of the concentrate.

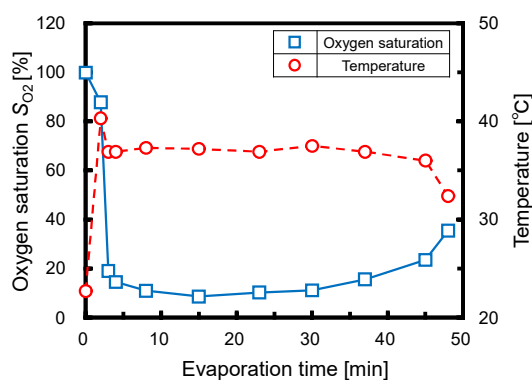


**Figure 10.** Temporal changes in the oxygen saturation  $S_{O_2}$  and temperature of a UFB dispersion in the evaporation flask.

It is an intriguing mystery how UFBs, which are supposed to be gaseous bubbles, can exist stably at about 10% of atmospheric pressure and temperatures of over 35 °C. The reason why UFBs can exist under the temperature and pressure at which water evaporates is unknown at present. As mentioned in the Introduction, such extreme stability of UFBs under the evaporation process has been reported: Jadhav and Barigou [7] concentrated UFB dispersions in a rotary evaporator for analysis. The fact that UFB dispersions can be evaporated underscores the need for further research, as well as expanding the range of methods for analyzing UFBs.

### 3.3. Size Measurement with Dynamic Light Scattering (DLS)

The concentrated samples can be analyzed using a variety of measurement techniques. We measured the size of concentrated UFBs using the dynamic light scattering (DLS) technique. Figure 11 shows the result of the DLS measurement: the autocorrelation function for a concentrated UFB dispersion whose concentration was  $10^{10}$  particles/mL. Although the initial concentration ( $10^9$  particles/mL) generated from the UFB generator did not provide sufficient scattering intensity for DLS ( $<3000$  cps), the 10-fold concentrated dispersion gave strong enough scattering intensity ( $>30$  kcps).

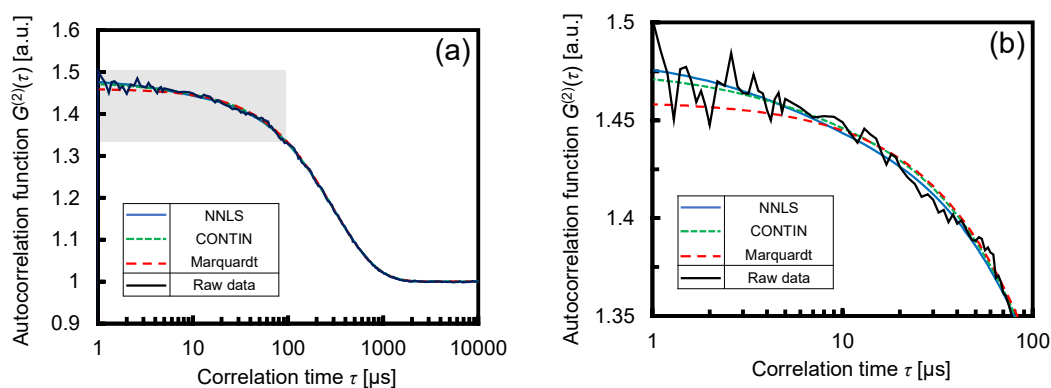


**Figure 11.** (a) Autocorrelation functions for the concentrated UFB dispersion with a number concentration of  $10^{10}$  particles/mL; (b) Enlarged view of (a) in the range of  $\tau \leq 100$   $\mu\text{s}$ .

It is a known fact that the particle size data differ depending on the algorithm used to analyze the raw data of autocorrelation function [26]. In addition to the ISO-standardized cumulant method, the ELSZ-1200 analysis software offers three other analysis algorithms: NNLS, CONTIN, and Marquardt. The raw data as well as the autocorrelation functions calculated by the three algorithms are shown in Figure 11. As shown in Figure 11a, the raw data and the calculations are in good agreement: looking over the functions in the entire range of  $1 \leq \tau \leq 10^5$   $\mu\text{s}$ , each algorithm appears to represent the raw data well. However, the magnified view shown in Figure 11b for  $\tau \leq 100$   $\mu\text{s}$  allows us to distinguish the subtle differences. Although the raw data contains noise, they show a downward curve from the y-intercept of about 1.5 a.u. The NNLS appears to best represent this trend in the range of  $\tau \leq 100$   $\mu\text{s}$ . This can be attributed to the characteristic of NNLS to resolve multiple exponential decays with high sensitivity.

Fitting the exponential decay of the autocorrelation function corresponding to a multimodal particle-dispersion system is a difficult problem; all algorithms have their advantages and disadvantages [27]. The NNLS method is the most sensitive of the three algorithms to fit multi-exponential decay, but it also has the disadvantage of being sensitive to noise [28]. On the contrary, the Marquardt method is the most insensitive and thus robust to noise, but it may miss the decay corresponding to the particles that should be present. Therefore, we should interpret the autocorrelation function by comparing the raw data with the fitted data in this way, because there is no “universal” algorithm suitable for any sample.

A closer look at the autocorrelation function makes it easier to interpret the reasons for the particle size distribution given by each algorithm. Figure 12 shows the size of the UFBs in intensity weighted and number weighted distribution. The DLS software calculated the intensity distribution using the viscosity and refractive index of water at 25  $^{\circ}\text{C}$ ; the number distribution was further calculated by assuming Rayleigh–Gans–Debye approximation. The conversion from intensity distribution to number distribution is a standard feature of the software of the DLS instrument used (ELSZ-1200).

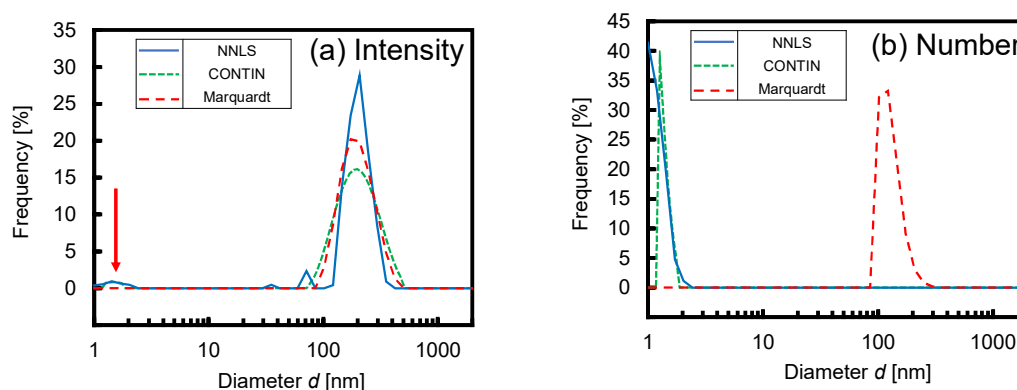


**Figure 12.** Size distributions of UFBs determined by the algorithms: (a) Intensity distribution; (b) Number distribution.

As expected, the three algorithms gave different particle size distributions. NNLS and CONTIN resolved multiple peaks, whereas Marquardt did only one. This difference is due to how many decays are assumed in the exponential fit to the autocorrelation function [27]. NNLS fitted the most decays and thus resolved most peaks, whereas CONTIN, which is more constrained than NNLS [28], resolved only the two main peaks. The peaks around 200 nm, which are common to all three analysis algorithms, are thought to represent particles measured by PTA, i.e., UFBs. The peak sizes are also consistent with the z-average size of  $\sim 180$  nm obtained by the cumulant method. This particle size range around 200 nm corresponds to the decay of the autocorrelation function in the range of  $10 \leq \tau \leq 1000 \mu\text{s}$ .

The identity of the peak indicated by the arrow in Figure 12a is not clear. The peaks around 2 nm given by the relatively sensitive algorithms (NNLS and CONTIN) may be related to the fact that the autocorrelation functions of the two algorithms had larger y-intercepts than that of the Marquardt algorithm; the y-intercept of Marquardt was about 1.46 a.u., while those of others were above 1.47 a.u. Thus, NNLS and CONTIN may have captured the early decay of the raw data. Note that the scattering intensity is approximately proportional to the number concentration  $N$  and the sixth power of diameter  $d^6$ . This is the reason why the peak around 2 nm is large in NNLS and CONTIN in Figure 12b. It is not clear whether 2-nm particles exist in the UFB dispersion. However, the raw data of the autocorrelation function shown in Figure 11b seems to indicate that a fast decay did indeed occur. Therefore, we cannot rule out the possibility that some kind of particles or small molecules exists in the nanometer range.

Table 2 summarizes the data for the peaks determined by the DLS measurement. The data obtained by PTA (mode diameter) are also shown in the table. Note that since the cumulant method does not provide any size distribution, the z-average diameter is not peak size. The peaks of the Marquardt method and PTA are in particularly good agreement with each other. Therefore, it is sufficient to conclude that the particle size distributions obtained by PTA and DLS are comparable depending on the choice of algorithm.

**Table 2.** Peaks determined by PTA and DLS.

Method	Algorithm	Intensity Weighted Size [nm] <sup>1</sup>	Number Weighted Size [nm] <sup>1</sup>
DLS	Cumulant	$179 \pm 0.5$	n/a
	NNLS	$196 \pm 9^2$	$1.6 \pm 0.1^2$
	CONTIN	$209 \pm 2^2$	$1.5 \pm 0.1^2$
	Marquardt	$203 \pm 2$	$135 \pm 7$
PTA	—	n/a	$135 \pm 5$

<sup>1</sup> Mean  $\pm$  standard deviation; <sup>2</sup> Primary peak.

#### 4. Conclusions

We investigated the effect of dilution and concentration, which are basic operations essential for analytical purposes, on the stability of ultrafine bubbles (UFBs). UFBs in ultrapure water were produced with air in a commercial generator. The number concentration and size of UFBs were quantified using a particle tracking analysis (PTA) instrument. The results showed that the UFB dispersion can be diluted with ultrapure water without losing the stability of UFBs, regardless of the dissolved gas concentration of the diluent; the number concentrations showed excellent linearity and the particle size distributions were unchanged. A rotary evaporator was also used to concentrate the UFB dispersion. The UFB dispersion was concentrated as calculated from the evaporated volume, i.e., the balance of the number of UFBs was established. In addition, evaporation did not change the size distribution of UFBs. The concentrated UFB dispersions reached a concentration of more than  $10^{10}$  particles/mL, which was sufficient to allow for measurement by dynamic light scattering (DLS). Using the concentrated dispersion, we discussed the importance of the selection of the algorithm for analyzing the raw data, i.e., autocorrelation function, in DLS. Among the algorithms implemented in the DLS instrument used, the peak analyzed by the Marquardt method gave the best agreement with the peak obtained by the PTA method.

**Author Contributions:** Conceptualization, K.T.; Methodology, Y.N. and S.T.; Validation, S.T.; Formal Analysis, Y.N.; Investigation, Y.N. and S.T.; Data Curation, S.T.; Writing—Original Draft Preparation, S.T. and Y.N.; Writing—Review & Editing, K.T. and S.F.; Visualization, S.T.; Supervision, K.T. and S.F. All authors have read and agreed to the published version of the manuscript.

**Funding:** This work was partially supported by JSPS KAKENHI Grant Number 20H02508.

**Conflicts of Interest:** The authors declare no conflict of interest.

#### Appendix A

Assuming that all the air-UFBs in water are dissolved as dissolved oxygen and nitrogen, the concentration of dissolved oxygen was calculated as follows. This is what was mentioned in Section 3.1.

If a gaseous UFB with a diameter of  $d$  is present in water, the number of moles of gas in the spherical UFB can be calculated by Equation (A1), assuming the ideal gas law, i.e.,  $PV = nRT$ :

$$n = \frac{PV}{RT} = \frac{(P_{\text{atm}} + \frac{4\sigma}{d}) \left( \frac{\pi d^3}{6} \right)}{RT} \quad (\text{A1})$$

where  $n$  is the number of moles of the gas,  $R$  is the gas constant,  $T$  is the absolute temperature,  $P_{\text{atm}}$  is the atmospheric pressure, and  $\sigma$  is the gas–liquid interfacial tension. Note that the bubble internal pressure  $P$  was calculated using the Laplace equation, i.e.,  $\Delta P = 4\sigma/d$ .

Assuming that all the gas in the UFB are dissolved in the liquid and the concentration of UFBs is  $N$  [particles/mL], the molar concentration  $c$  [mol/L] and mass concentration  $C$  [mg/L] can be calculated as follows:

$$c = nN \frac{1000 \text{ mL}}{1 \text{ L}} \quad (\text{A2})$$

$$C = cM \times \frac{1000 \text{ mg}}{1 \text{ g}} \quad (\text{A3})$$

where  $M$  [g/mol] is the molar mass of the gas.

Assuming that the gas in the UFBs is air (21 vol%  $\text{O}_2$ ), the calculations of  $c$  and  $C$  of dissolved oxygen can be performed as follows:

$$c = \frac{\left( 101.3 \times 10^3 + \frac{4 \times 0.072}{200 \times 10^{-9}} \right) \left[ \frac{\pi (200 \times 10^{-9})^3}{6} \right]}{8.31 \times 298} \times 10^9 \times 1000 \times 0.21 = 5.5 \times 10^{-7} \text{ mol/L} \quad (\text{A4})$$

$$C = 5.5 \times 10^{-7} \times 32 \times 1000 = 0.018 \text{ mg/L} \quad (\text{A5})$$

The following values were substituted into the calculation:  $\pi = 3.14$ ,  $d = 200 \text{ nm}$ ,  $P_{\text{atm}} = 101.3 \text{ kPa}$ ,  $\sigma = 72 \text{ mN/m}$ ,  $R = 8.31 \text{ J/(mol}\cdot\text{K)}$ ,  $T = 298 \text{ K}$ ,  $N = 10^9 \text{ particles/mL}$ ,  $M = 32 \text{ g/mol}$ .

## References

- ISO 20480-1:2017. *Fine Bubble Technology—General Principles for Usage and Measurement of Fine Bubbles—Part 1: Terminology*; International Organization for Standardization (ISO): Genève, Switzerland, 2017. Available online: <https://www.iso.org/standard/68187.html?browse=tc> (accessed on 1 August 2020).
- Alheshibri, M.; Qian, J.; Jehannin, M.; Craig, V.S.J. A History of Nanobubbles. *Langmuir* **2016**, *32*, 11086–11100. [[CrossRef](#)] [[PubMed](#)]
- Azevedo, A.; Oliveira, H.; Rubio, J. Bulk Nanobubbles in the Mineral and Environmental Areas: Updating Research and Applications. *Adv. Colloid Interface Sci.* **2019**, *271*, 101992. [[CrossRef](#)] [[PubMed](#)]
- Alheshibri, M.; Craig, V.S.J. Differentiating between Nanoparticles and Nanobubbles by Evaluation of the Compressibility and Density of Nanoparticles. *J. Phys. Chem. C* **2018**, *122*, 21998–22007. [[CrossRef](#)]
- Alheshibri, M.; Jehannin, M.; Coleman, V.A.; Craig, V.S.J. Does Gas Supersaturation by a Chemical Reaction Produce Bulk Nanobubbles? *J. Colloid Interface Sci.* **2019**, *554*, 388–395. [[CrossRef](#)]
- Alheshibri, M.; Craig, V.S.J. Generation of Nanoparticles upon Mixing Ethanol and Water; Nanobubbles or Not? *J. Colloid Interface Sci.* **2019**, *542*, 136–143. [[CrossRef](#)]
- Jadhav, A.J.; Barigou, M. Bulk Nanobubbles or Not Nanobubbles: That is the Question. *Langmuir* **2020**, *36*, 1699–1708. [[CrossRef](#)]
- Tantra, R.; Schulze, P.; Quincey, P. Effect of Nanoparticle Concentration on Zeta-potential Measurement Results and Reproducibility. *Particuology* **2010**, *8*, 279–285. [[CrossRef](#)]
- Tuziuti, T.; Yasui, K.; Kanematsu, W. Influence of Addition of Degassed Water on Bulk Nanobubbles. *Ultrason. Sonochem.* **2018**, *43*, 272–274. [[CrossRef](#)]
- Terasaka, K.; Himuro, S.; Ando, K.; Hata, T. *Introduction to Fine Bubble Science and Technology*; Nikkan Kogyo Shimbun, Ltd.: Tokyo, Japan, 2016; ISBN 9784526076251.
- IDEC Global. Ultrafine Bubble Generation Technology. Available online: <https://www.idec.com/home/finebubble/index.html> (accessed on 1 September 2020).
- Filipe, V.; Hawe, A.; Jiskoot, W. Critical Evaluation of Nanoparticle Tracking Analysis (NTA) by NanoSight for the Measurement of Nanoparticles and Protein Aggregates. *Pharm. Res.* **2010**, *27*, 796–810. [[CrossRef](#)]
- ISO 19430:2016. *Particle Size Analysis—Particle Tracking Analysis (PTA) Method*; International Organization for Standardization (ISO): Genève, Switzerland, 2016. Available online: <https://www.iso.org/standard/64890.html> (accessed on 23 October 2020).
- Gross, J.; Sayle, S.; Karow, A.R.; Bakowsky, U.; Garidel, P. Nanoparticle Tracking Analysis of Particle Size and Concentration Detection in Suspensions of Polymer and Protein Samples: Influence of Experimental and Data Evaluation Parameters. *Eur. J. Pharm. Biopharm.* **2016**, *104*, 30–41. [[CrossRef](#)]
- ISO 22412:2017. *Particle Size Analysis—Dynamic Light Scattering (DLS)*; International Organization for Standardization (ISO): Genève, Switzerland, 2017. Available online: <https://www.iso.org/standard/65410.html> (accessed on 1 August 2020).
- Provencher, S.W. Contin: A General Purpose Constrained Regularization Program for Inverting Noisy Linear Algebraic and Integral Equations. *Comput. Phys. Commun.* **1982**, *27*, 229–242. [[CrossRef](#)]
- Lawson, C.L.; Hanson, R.J. *Solving Least Squares Problems*; Prentice-Hall series in automatic computation; Prentice-Hall: Englewood Cliffs, NJ, USA, 1974; ISBN 9780138225858.
- Marquardt, D.W. An Algorithm for Least-Squares Estimation of Nonlinear Parameters. *J. Soc. Ind. Appl. Math.* **1963**, *11*, 431–441. [[CrossRef](#)]
- Nirmalkar, N.; Pacek, A.W.; Barigou, M. Interpreting the Interfacial and Colloidal Stability of Bulk Nanobubbles. *Soft Matter* **2018**, *14*, 9643–9656. [[CrossRef](#)]
- Häbich, A.; Ducker, W.; Dunstan, D.E.; Zhang, X. Do Stable Nanobubbles Exist in Mixtures of Organic Solvents and Water? *J. Phys. Chem. B* **2010**, *114*, 6962–6967. [[CrossRef](#)]
- Uchida, T.; Yamazaki, K.; Gohara, K. Generation of Micro- and Nano-bubbles in Water by Dissociation of Gas Hydrates. *Korean J. Chem. Eng.* **2016**, *33*, 1749–1755. [[CrossRef](#)]

22. Uchida, T.; Liu, S.; Enari, M.; Oshita, S.; Yamazaki, K.; Gohara, K. Effect of NaCl on the Lifetime of Micro- and Nanobubbles. *Nanomaterials* **2016**, *6*, 31. [[CrossRef](#)]
23. Oh, S.H.; Kim, J. Generation and Stability of Bulk Nanobubbles. *Langmuir* **2017**, *33*, 3818–3823. [[CrossRef](#)]
24. Weijs, J.H.; Seddon, J.R.T.; Lohse, D. Diffusive Shielding Stabilizes Bulk Nanobubble Clusters. *ChemPhysChem* **2012**, *13*, 2197–2204. [[CrossRef](#)]
25. Yasui, K.; Tuziuti, T.; Kanematsu, W.; Kato, K. Dynamic Equilibrium Model for a Bulk Nanobubble and a Microbubble Partly Covered with Hydrophobic Material. *Langmuir* **2016**, *32*, 11101–11110. [[CrossRef](#)]
26. Franks, K.; Kestens, V.; Braun, A.; Roebben, G.; Linsinger, T.P.J. Non-Equivalence of Different Evaluation Algorithms to Derive Mean Particle Size from Dynamic Light Scattering Data. *J. Nanopart. Res.* **2019**, *21*, 195. [[CrossRef](#)]
27. Russo, P. A Practical Minicourse in Dynamic Light Scattering. Available online: [http://www.eng.uc.edu/~beaucag/Courses/Characterization/DLS/PaulRussoLSU2012DLS\\_Minicourse.pdf](http://www.eng.uc.edu/~beaucag/Courses/Characterization/DLS/PaulRussoLSU2012DLS_Minicourse.pdf) (accessed on 1 August 2020).
28. Stetefeld, J.; McKenna, S.A.; Patel, T.R. Dynamic Light Scattering: A Practical Guide and Applications in Biomedical Sciences. *Biophys. Rev.* **2016**, *8*, 409–427. [[CrossRef](#)] [[PubMed](#)]

**Publisher's Note:** MDPI stays neutral with regard to jurisdictional claims in published maps and institutional affiliations.



© 2020 by the authors. Licensee MDPI, Basel, Switzerland. This article is an open access article distributed under the terms and conditions of the Creative Commons Attribution (CC BY) license (<http://creativecommons.org/licenses/by/4.0/>).